Adsorption and desorption of crystal violet and basic red 9 by multi-walled carbon nanotubes

Xian Chen and Ching-Ju Monica Chin

ABSTRACT

Batch adsorption and desorption of crystal violet (CV) and basic red 9 (BR9) on multi-walled carbon nanotubes (MWCNTs) were conducted. To investigate the possible mechanisms of adsorption/desorption hysteresis, oxidized MWCNTs (O-MWCNTs) with more oxygen-containing groups were obtained by oxidizing as-purchased MWCNTs (A-MWCNTs) using nitric acid. The adsorption kinetics could be described by the pseudo-second-order model, suggesting that chemical reactions are the rate-limiting steps. The adsorption isotherms were fitted well by the Langmuir model, which suggests that, in addition to π–π interactions, chemical reactions significantly affect the adsorption. The adsorption capacity decreased in the order of CV on A-MWCNTs, BR9 on A-MWCNTs, and BR9 on O-MWCNTs, possibly because the amidation between BR9 and the surface groups of MWCNTs results in steric hindrance, which limits the adsorption of BR9 to inner grooves between CNT bundles. Adsorption/desorption hysteresis was observed for BR9 but not for CV. It was found that the π–π interaction and molecular entrapment were not responsible for the adsorption/desorption hysteresis. The hysteresis might be caused by the irreversible amide bonds between BR9 and MWCNTs. The results indicate that the steric hindrance due to the three-dimensional structure of organic compounds plays an important role in both adsorption/desorption kinetics and equilibria.

Key words | adsorption/desorption hysteresis, amide bond, Langmuir model, steric hindrance

Xian Chen
Ching-Ju Monica Chin (corresponding author)
Graduate Institute of Environmental Engineering,
National Central University,
300 Jungda Rd., Jungli, Taoyuan, 32001,
Taiwan
E-mail: *cjchin@cc.ncu.edu.tw*

INTRODUCTION

Adsorption of organic compounds on carbon nanotubes (CNTs) has been investigated intensively to understand the fate and transport of CNTs (Wang *et al.* 2010a; Yang *et al.* 2010; Apul & Karanfil 2015). The mechanisms of adsorption of organic compounds by CNTs can be divided into nonspecific interactions and conditional attractive forces. Nonspecific interactions, which are generally referred to as van der Waals interactions, are the major contributors of overall attractive forces (Apul & Karanfil 2015). π–π interactions between aromatic compounds and the surface of CNTs have been considered as the major mechanism. Other attractions include hydrogen bonding between functional groups of organic compounds and CNT surfaces and electrostatic interactions between ionic compounds and surface charges of CNTs.

Compared to the literature on adsorption, the literature on the desorption behaviors of organic compounds from CNTs is scarce, and the topic still requires further investigation (Yang & Xing 2007; Oleszczuk *et al.* 2009; Yang *et al.* 2010; Ma *et al.* 2011; Wu *et al.* 2013). The strong π–π interaction between tetra-tert-butylphthalocyanines and CNT surface has been proposed as a possible mechanism for desorption hysteresis (Wang *et al.* 2002). After adsorption of organic compounds, rearrangement of CNT bundles may lead to desorption hysteresis, which has been observed for the adsorption of organic compounds with polar functional groups on CNTs, such as bisphenol A, 17α-ethinyl estradiol, oxytetracycline, carbamazepine, norfloxacin, (Pan *et al.* 2008; Oleszczuk *et al.* 2009; Wang *et al.* 2010b), and polycyclic aromatic hydrocarbons on fullerene (Yang & Xing 2007). Wu *et al.* (2013) has concluded that the desorption hysteresis of aniline and 4-methylaniline on oxidized-MWCNTs is due to the irreversible amide bonding (i.e. –CONH) between the amino groups of anilines and the functional groups on MWCNTs. Desorption of organic compounds from CNTs is as important as adsorption for evaluating environmental and health risks of both CNTs and contaminants.

doi: 10.2166/wst.2019.157

In general, the underlying mechanisms of desorption and desorption hysteresis from CNTs are mostly discussed by adsorption and desorption isotherms only. The adsorption and desorption kinetics should also be considered for the interpretation of desorption hysteresis. The objectives of this work were to investigate the adsorption/desorption of organic compounds from MWCNTs and to examine the mechanisms for adsorption/desorption hysteresis. Crystal violet (CV) and basic red 9 (BR9) were used to understand the influences of the structures of molecules and the functional groups on the adsorption and desorption of organic compounds on MWCNTs. Both the kinetics and the isotherms of adsorption and desorption were determined.

MATERIALS AND METHODS

Oxidation and characterization of MWCNTs

The MWCNTs (US Research Nanomaterials, Inc.) have an outer diameter of 50–80 nm and an inner diameter of 5–15 nm, according to the manufacturer. To increase the amount of surface oxygen functional groups, the as-purchased MWCNTs (A-MWCNTs) were oxidized. A-MWCNTs were dispersed in 500 mL of 3 M nitric acid and sonicated for 30 min. Then, the MWCNTs dispersion was refluxed at 120 °C for 3 h with stirring. After being cooled to room temperature, the MWCNTs were separated from nitric acid by filtration and the oxidized MWCNTs were washed by deionized water repeatedly until the pH value of the filtrate was approximately 6 (Chin *et al.* 2010). The as-purchased and oxidized MWCNTs are referred to as A- and O-MWCNTs, respectively, in the following text.

Nitrogen adsorption and desorption on the MWCNTs were conducted at 77 K in an accelerated surface area and porosimetry system (ASAP, ASAP2010, Micrometrics Inc.). The surface area and the pore size distribution were then obtained by analyzing the nitrogen adsorption–desorption isotherms using Brunauer-Emmett-Teller (BET) and Barrett-Joyner-Halenda (BJH) models. Fourier transform infrared spectroscopy (FTIR, JASCO, FT/IR-4600) was used to characterize the surface groups on the MWCNTs.

Batch adsorption and desorption

The adsorption/desorption kinetics and isotherms were studied by batch experiments in screw cap centrifuge tubes with Teflon liners. CV (Sigma-Aldrich) and BR9 (Sigma-Aldrich) were dissolved in a background solution containing 0.01 M $CaCl_2$ (Merck) and 200 mg/L NaN_3 (as a biocide, Merck) in deionized water. The pH values of the suspensions were adjusted to 8.0 ± 0.2 by 0.01 M HCl and 0.01 M NaOH. MWCNTs (10 mg) were dispersed in 6.5 ml CV or BR9 solution. For adsorption kinetic study, the initial concentration of CV or BR9 was 100 mg/L. The samples were taken at 5, 10, 20, 30 40, 60, 120, and 240 min. For adsorption/desorption isotherms, the initial concentrations were 20, 50, 100, 150, 200, 150, 300, 350 and 400 mg/L. All experiments were conducted in a reciprocal shaker with a rotation speed of 120 rpm at room temperature (25 ± 1 °C). The experiments were shielded from light to avoid photolysis of CV and BR9, and blank experiments without addition of MWCNTs were also conducted to confirm that the concentration decrease was solely due to adsorption on MWCNTs.

Desorption experiments were conducted immediately after adsorption reached equilibrium. For the desorption kinetic study, the supernatant was removed and displaced by the same volume of background solution at the same time interval as the adsorption kinetic study. The tubes were resealed and shaken. The MWCNTs suspension was centrifuged at 6,000 rpm for 10 min before withdrawing the supernatant. The concentrations of CV and BR9 in the supernatant were determined by UV-Vis spectrophotometer (Jasco, V-650). The absorbance bands of CV and BR9 are 590 and 540 nm, respectively. All adsorption and desorption experiments were at least duplicated.

Data analysis

The pseudo-first-order, pseudo-second-order, Elovich, and intraparticle diffusion models were used to fit the adsorption kinetic data. The mathematical expressions are given in Equations (1)–(4), respectively (Weber & Morris 1963; Lagergren 1998; Mckay *et al.* 1999; Shek *et al.* 2009).

$$\ln(q_e - q_t) = \ln(q_e) - k_1 t \tag{1}$$

$$\frac{t}{q_t} = \frac{1}{k_2 q_e^2} + \frac{1}{q_e} t \tag{2}$$

$$q_t = \frac{1}{\beta} \ln(\alpha\beta) + \frac{1}{\beta} \ln t \tag{3}$$

$$q_t = k_i t^{0.5} \tag{4}$$

Here, q_e and q_t are the amounts of adsorbate on adsorbent (mg/g) at equilibrium and at time t (min), respectively, and k_1 is the pseudo-first-order rate constant

(1/min). k_2 is the pseudo-second-order rate constant (g/mg·min). α (mg/g·min) and β (g/mg) are constants for the Elovich model. k_i is the rate constant (mg/g·min$^{0.5}$) for the intraparticle diffusion model.

The Langmuir, Freundlich, and Temkin models have been used to describe the adsorption isotherm, and the equations are shown in Equations (5)–(7), respectively (Pan *et al.* 2008; Kuo 2009; Oleszczuk *et al.* 2009).

$$q_e = \frac{q_{max} C_e}{C_e + \frac{q_{max}}{K_L}} \tag{5}$$

$$q_e = K_F C_e^{1/n} \tag{6}$$

$$q_e = K_1 \ln K_2 + K_1 \ln C_e \tag{7}$$

Here, K_L is the parameter of the Langmuir model and q_{max} is the maximum amount of adsorption. K_F and n are the parameters for the Freundlich model. K_1 and K_2 are the coefficients of the Temkin model.

To quantify the desorption hysteresis, the adsorption/desorption hysteresis index (HI) was applied in this study (Huang *et al.* 1998). The equation can be written as

$$\mathrm{HI} = (q_e^d - q_e^a)/q_e^a|_{T, C_e} \tag{8}$$

where q_e^a and q_e^d are amounts of adsorbate on adsorbent at equilibrium during adsorption and desorption, respectively. T (°C) and C_e (mg/L) specify the constant temperature and the equilibrium concentration of solute, respectively.

RESULTS AND DISCUSSION

Characterization of MWCNTs

Table 1 gives the micropore area, external surface area, BET surface area and micropore volume obtained by analyzing the adsorption/desorption of nitrogen on the MWCNTs at 77 K. The BET surface area of A-MWCNTs increases from 87.98 m^2/g to 97.69 m^2/g after HNO_3 treatment. The external surface area, which is mainly attributed to groove and interstitial sites of CNT bundles (Agnihotri *et al.* 2005), increases from 73.89 m^2/g to 82.69 m^2/g (11.9%). The increase in external surface area may be caused by the damage of surface structure of A-MWCNTs after HNO_3 treatment. The pore size distributions of A- and O-MWCNTs are given in Figure S1 (available with the online version of this paper).

Table 1 | Surface properties of A-MWCNTs and O-MWCNTs

	Micropore area (m^2/g)	External surface area (m^2/g)	BET surface area (m^2/g)	Micropore volume (cm^3/g)
A-MWCNTs	14.09	73.89	87.98	0.006562
O-MWCNTs	15.00	82.69	97.69	0.006894

Figure 1 shows the FTIR spectra of A-MWCNTs and O-MWCNTs. Bands can be observed at approximately 1,500 cm^{-1} and 2,400 cm^{-1} on both A-MWCNTs and O-MWCNTs. The bands at 1,550–1,650 cm^{-1} represent the –C = O from the acidic group, and those at 2,300–2,400 represent the –OH stretch from strongly H-bonded –COOH (Salam & Burk 2008; Kuo 2009). Additionally, these two bands of O-MWCNTs are distinctly larger than those of A-MWCNTs, which suggests that HNO_3 treatment increases the oxygen-containing functional groups on the surface of A-MWCNTs. Previous work has also shown that the amount of oxygen-containing groups on CNTs can be increased by the same oxidation process (Chin *et al.* 2010; Chi *et al.* 2016).

Adsorption kinetics

The adsorption kinetics of CV on A-MWCNTs and BR9 on A-MWCNTs and O-MWCNTs are shown in Figure 2. The amounts of adsorption increase significantly in the first 10 min and then slow down. There were no significant changes in the adsorption amounts of dyes after 50 min for CV on A-MWCNTs and for BR9 on O-MWCNTs. The adsorption of BR9 on A-MWCNTs increased slowly until approximately 120 min. Therefore, all of the adsorption isotherm experiments were conducted for 120 min.

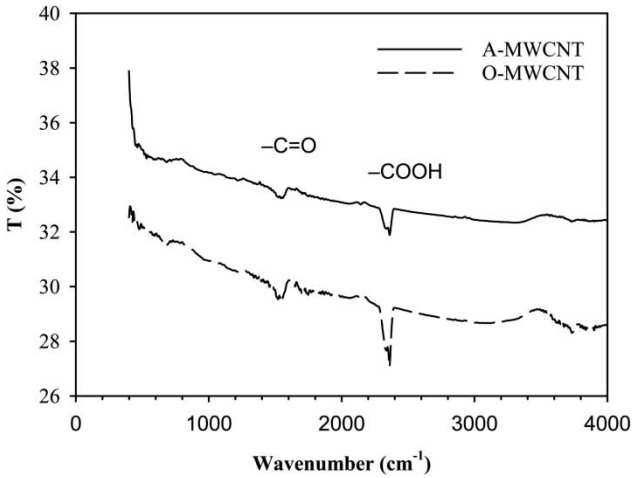

Figure 1 | FTIR spectra of A- and O-MWCNTs.

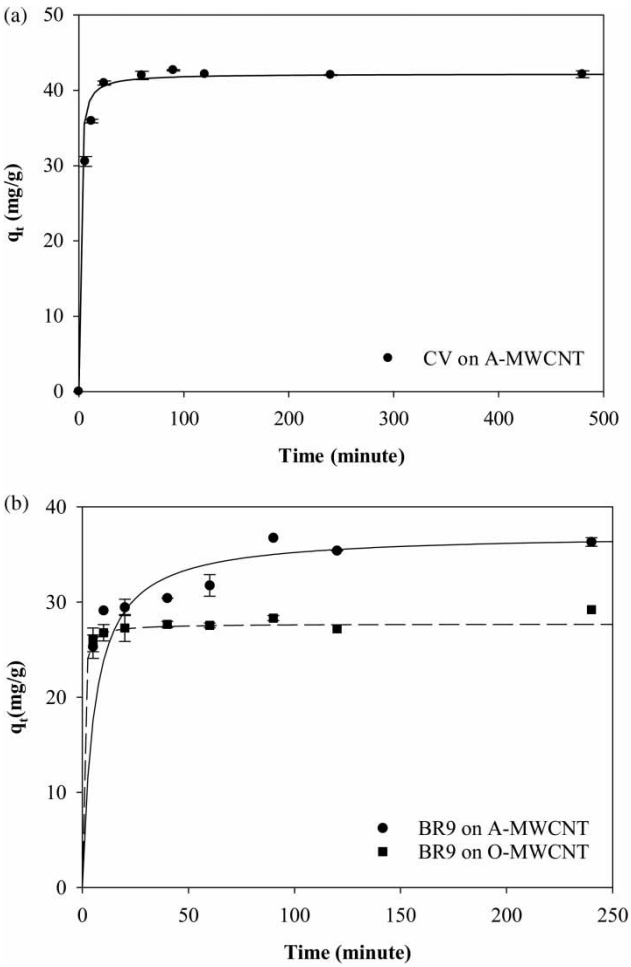

Figure 2 | Adsorption kinetics of (a) CV on A-MWCNTs and (b) BR9 on both MWCNTs. The solid lines represent the model fitting by the pseudo-second-order equation. Initial concentration = 100 mg/L.

The adsorption of CV by A-MWCNTs or BR9 by A- and O-MWCNTs reached equilibrium much faster than reported in the literature (Oleszczuk *et al.* 2009), and the two-stage adsorption (i.e. fast initial adsorption on outer surfaces and slow diffusion to interlayers and micropores) was not observed. The pores in MWCNTs used in this study are mainly composed of mesopores, as shown in Figure S1(a), so that the slow diffusion of dye into interlayers and micropores was apparently negligible. In addition, CV and BR9 molecules are approximately 1 nm (estimated by bond lengths), which are larger than the main size of micropores of A-MWCNTs and O-MWCNTs (0.69 nm and 0.68 nm, respectively, as shown in Figure S1(b)). This means that most of the micropores are not available for CV or BR9. Therefore, the adsorption process for dyes on both A-MWCNTs and O-MWCNTs can be considered as fast adsorption.

The kinetic data were also fitted by the pseudo-first-order, pseudo-second-order, Elovich, and intraparticle diffusion models. The fitted kinetic parameters of all four models are shown in Table 2. The R^2 values for the pseudo-first-order, Elovich, and intraparticle diffusion models are less than 0.95, which means that the adsorptions of CV and BR9 onto MWCNTs do not follow these three models. The regression coefficients of CV on A-MWCNTs, BR9 on A-MWCNTs, and BR9 on O-MWCNTs fitted by the pseudo-second-order model are 1.000, 0.998, and 0.999, respectively. The comparison of experimental data and fitting results of four models are shown in Figure S2 (available with the online version of this paper). The results agree with the literature (Sabna *et al.* 2016) and suggest that the interaction between CV, as well as BR9, and the surface of MWCNTs is the rate-limiting step (Ho & McKay 1999).

Adsorption isotherm

Figure 3 shows that the adsorption capacity of CV on A-MWCNTs is the highest. The adsorption capacity of BR9 on A-MWCNTs is higher than that on O-MWCNTs. The Langmuir, Freundlich, and Temkin models have been used to fit the experimental data. Table 3 shows the fitted adsorption isotherm parameters and regression coefficients. Although all three models show good correlations to the

Table 2 | Model fitting results of the kinetic for adsorption of CV and BR9 on MWCNTs. (A) and (O) refer to A-MWCNTs and O-MWCNTs, respectively

Pseudo-first-order	**k_1 (1/min)**		**R^2**
CV	0.0047		0.388
BR9 (A)	0.0140		0.973
BR9 (O)	0.0092		0.277
Pseudo-second-order	**q_e (mg/g)**	**k_2 (g/mg·min)**	**R^2**
CV	42.19	0.0252	1.000
BR9 (A)	37.17	0.0048	0.998
BR9 (O)	27.70	0.0951	0.999
Elovich	**β (g/mg)**	**α (mg/g·min)**	**R^2**
CV	0.420	7.542×10^5	0.678
BR9 (A)	0.320	1.914×10^3	0.902
BR9 (O)	0.923	1.910×10^9	0.770
Intra-particle diffusion	**k_i (mg/g·min$^{0.5}$)**		**R^2**
CV	0.4133		0.396
BR9 (A)	0.8616		0.808
BR9 (O)	0.3459		0.604

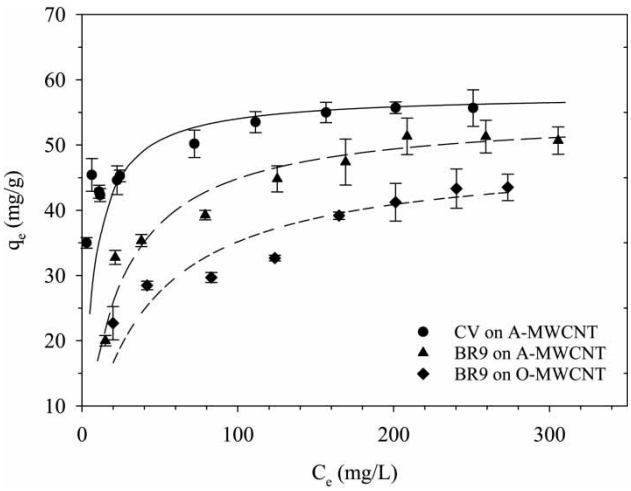

Figure 3 | Adsorption isotherms of CV on A-MWCNTs and BR9 on A-MWCNTs and O-MWCNTs at 25 °C. The solid lines represent the fittings by the Langmuir model.

Table 3 | Model fitting results of the isotherms for adsorption of CV and BR9 on MWCNTs

Langmuir	q_{max} (mg/g)	K_L (L/g)	R^2
CV (A)	57.80	6.97	0.999
BR9 (A)	55.55	2.35	0.994
BR9 (O)	48.78	1.26	0.981
Freundlich	K_F (L/g)$^{1/n}$	**1/n**	R^2
CV (A)	33.66	0.0947	0.973
BR9 (A)	17.75	0.1919	0.979
BR9 (O)	10.58	0.2511	0.953
Temkin	K_1 (L/mg)	K_2	R^2
CV (A)	4.785	548.05	0.975
BR9 (A)	7.955	2.38	0.963
BR9 (O)	8.165	0.68	0.926

experimental results, the Langmuir model has the highest R^2 values (i.e. 0.999 for CV on A-MWCNTs, 0.994 for BR9 on A-MWCNTs, and 0.981 for BR9 on O-MWCNTs). Similar fitting results were found in the adsorption of CV on nanocables (Liu *et al.* 2015) and on magnetic-modified MWCNTs (Madrakian *et al.* 2011).

According to Table 3, the adsorption capacities of CV on A-MWCNTs, BR9 on A-MWCNTs, and BR9 on O-MWCNTs are 57.80 mg/g, 55.55 mg/g, and 48.78 mg/g, respectively. The hydrophobic force, which can be described by log K_{ow}, is another potential interaction affecting adsorption. Organic compounds with higher log K_{ow} are more hydrophobic and may have higher tendencies to be adsorbed by MWCNTs. The log K_{ow} values of CV and BR9 are 0.51 and −0.21, respectively (Tsai *et al.* 1991). Thus, the adsorption amount of CV on A-MWCNTs is greater than those of BR9 on both A- and O-MWCNTs.

The π–π interaction has been considered as the major mechanism for the adsorption of aromatic compounds on CNTs (Lin & Xing 2008). In this study, CV and BR9 both contain three aromatic rings; however, the strength of the π–π interaction between them and MWCNTs may not be as strong, due to their 3D structures. Aromatic compounds with planar structure, such as polycyclic aromatic hydrocarbons, can match the array of hexagonal carbon rings on the surface of MWCNTs well (Gotovac *et al.* 2007). However, with their three-dimensional structures, the three benzene rings of CV and BR9 cannot lie flat on the surfaces of MWCNTs. Hence, the π–π interaction between adsorbate and adsorbent may be relatively weak in this study as compared to the literature (Gotovac *et al.* 2007; Lin & Xing 2008).

The terminal functional groups of CV and BR9 molecules are $-N-(CH_3)_2$ and $-NH_2$, respectively. Both $-N(CH_3)_2$ and $-NH_2$ are electron-donating groups which can enhance the density of π-electrons and increase the strength of π–π interactions. The adsorption capacity of CV is higher than that of BR9, which suggests that the electron-donor-acceptor reaction does not significantly influence the adsorption of CV and BR9 by MWCNTs. Furthermore, the pH values were adjusted to 8 to avoid protonation of the $-NH_2$ on BR9 so that the electrostatic interaction might not come into play.

Wu *et al.* (2013) observed an irreversible amidation reaction between the amino groups of anilines and the carboxyl/lactonic groups (−COOH/−COOR) on the oxidized MWCNTs surfaces. BR9 contains two amino groups and one imino group, which could be considered as three aniline molecules connected to a carbon. From the FTIR spectra (Figure 1), there are carboxyl groups on the surfaces of both A-MWCNTs and O-MWCNTs. Therefore, the amidation may occur between the amino groups of BR9 and the carboxyl groups on MWCNTs. The amine groups of CV are tertiary: that is, there is no hydrogen bound to the nitrogen. There can thus be no amidation between CV and MWCNTs. Because only one of the three benzene rings can lie on the surface of the MWCNTs, and amidation prevents further interaction between BR9 and the MWCNTs, the adsorption is thus monolayer. Consequently, the Langmuir model describes the adsorption isotherm well.

The mesopores of A-MWCNTs and O-MWCNTs are mostly of diameters of 2–3 nm (Figure S1(a)), and the size of BR9 is approximately 1 nm (estimated by the bond lengths). Amidation between BR9 and the carboxyl groups

on MWCNTs might result in longer bond lengths than π–π interaction and lead to adjustment of BR9 for better adsorption position (Jin *et al.* 2015; Yu *et al.* 2017), which may result in loose packing of BR9 on MWCNTs and limit the transport of BR9 into the inner adsorption sites. Amidation cannot occur between CV and MWCNTs, because CV does not contain amino groups, and the adsorption of CV by MWCNTs may be only due to the π–π interaction. Without steric hindrance, CV might diffuse into the inner space. As a result, the adsorption capacity of CV is higher than that of BR9. Compared to A-MWCNTs, O-MWCNTs contain more carboxyl groups, which may provide more active sites for BR9, and the adsorption capacity may be higher. However, because O-MWCNTs contain more carboxyl groups, those BR9 molecules quickly adsorbed on the pore openings of the O-MWCNTs in the beginning stage may limit diffusion to deeper adsorption sites. Therefore, the adsorption of BR9 on O-MWCNTs reaches equilibrium faster than that on A-MWCNTs (Figure 2(b)), while the adsorption capacity of BR9 on O-MWCNTs is lower than that on A-MWCNTs.

Desorption of CV and BR9 from MWCNTs

The desorption kinetics of CV from A-MWCNT and BR9 from both A- and O-MWCNTs are illustrated in Figure S3 (available online). It requires approximately 100 min to reach desorption equilibrium for all three systems. Additionally, it is observed that the desorption of BR9 from O-MWCNTs reaches equilibrium slower than that from A-MWCNTs.

Desorption isotherms of CV on A-MWCNTs as well as BR9 on A-MWCNTs and O-MWCNTs are provided in Figure 4. No desorption hysteresis was observed for CV on A-MWCNTs, since the desorption and adsorption isotherms overlapped, while significant desorption hysteresis was observed for BR9 from both A-MWCNTs and O-MWCNTs.

Desorption hysteresis may be divided into true hysteresis and artificial hysteresis. Artificial hysteresis is caused by some external factors such as loss of adsorbent or adsorbate, degradation of adsorbate, and insufficient time for adsorption or desorption equilibrium. In this study, the suspension was adequately centrifuged after shaking, before analyzing the concentrations of CV and BR9, in order to avoid the loss of the MWCNTs. The losses of CV and BR9 were less than 3%, as confirmed by the blank experiments. All of the batch experiments were shielded from light to avoid the potential photodegradation of CV and BR9, and the biodegradation was controlled by adding 200 mg/L NaN_3 into the background solution. Additionally, the kinetic experiments showed that the adsorption or desorption reached equilibriums within 120 min. Therefore, the de-sorption hysteresis observed in this study should be considered as true hysteresis.

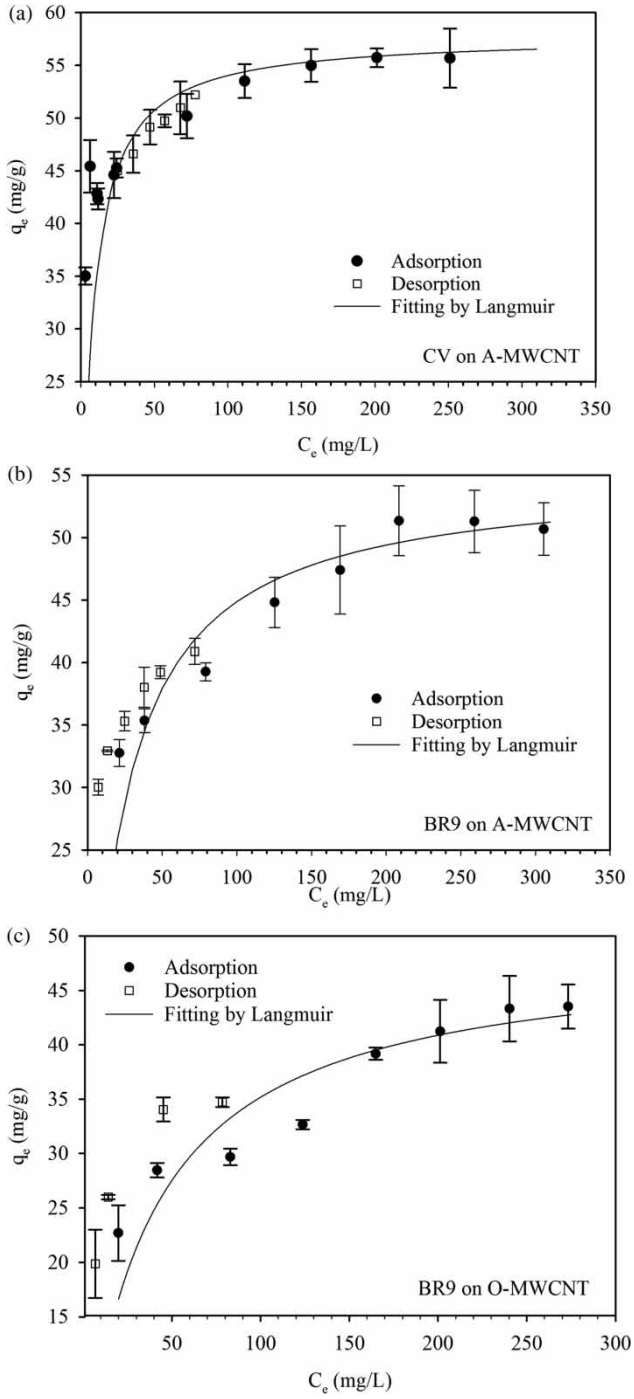

Figure 4 | Adsorption and desorption isotherms of (a) CV on A-MWCNTs, (b) BR9 on A-MWCNTs and (c) BR9 on O-MWCNTs. The solid lines represent the fittings by the Langmuir model.

Organic compounds with higher affinity to CNTs would be more likely to rearrange the bundles of CNTs and cause more significant desorption hysteresis (Ma *et al.* 2011). CV has higher affinity to the MWCNTs than does BR9; however, no adsorption/desorption hysteresis is observed. In addition, ultrasonication can significantly loosen the bundles of CNTs (Saleh *et al.* 2008). If adsorbed molecules were entrapped between bundled MWCNTs, ultrasonic treatment should increase the desorption. There was no significant change between desorption before and after ultrasonic treatment in all three conditions (Figure 5). Hence, the molecular entrapment made no contribution to the desorption hysteresis of BR9 on MWCNTs.

Strong π–π interaction has been proposed to represent the mechanism of immobilization of tetra-tert-butylphthalocyanines on CNT surfaces and to lead to desorption hysteresis (Wang *et al.* 2002). Both CV and BR9 might not be able to lie flat on the MWCNTs surface, and the π–π interaction would not be as strong as reported in the literature (Gotovac *et al.* 2007; Lin & Xing 2008) due to their 3-D structures. However, desorption hysteresis was only observed for BR9. Therefore, π–π interaction might not be the reason for the desorption hysteresis observed here.

It has been discussed that the adsorptions of BR9 on A-MWCNTs and O-MWCNTs were mainly due to the irreversible amidation between the amino groups of BR9 and the carboxyl groups on MWCNTs. Such amidation could not occur between CV and MWCNTs because CV has no amino groups. During desorption, some BR9 molecules are fixed by irreversible amidation, and the BR9 molecules adsorbed via π–π interaction might desorb and diffuse to the solution. Without irreversible amidation, all CV molecules easily desorb from MWCNTs: thus, the adsorption/desorption hysteresis was not observed.

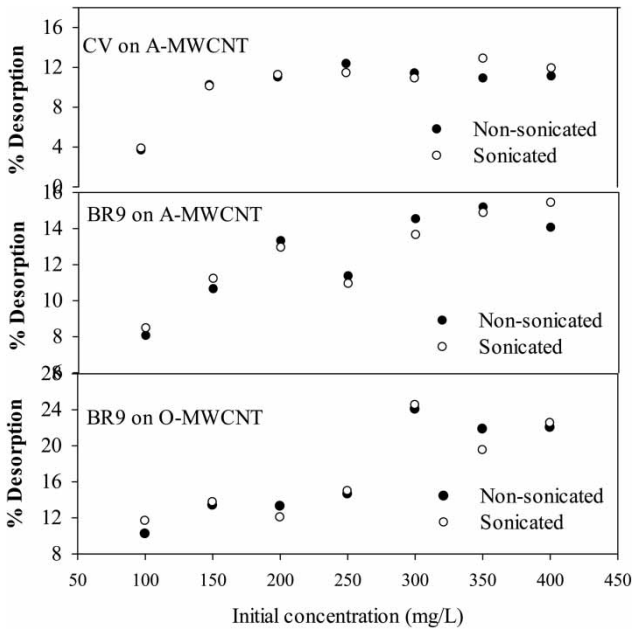

Figure 5 | Percentage of desorption with and without ultrasonic treatment.

The desorption HI value has been applied to compare the degree of desorption hysteresis (Huang *et al.* 1998). HI is defined as the ratio of the excessive adsorbed amount after desorption to the adsorbed amount during adsorption with respect to the specified equilibrium concentration. Higher HI values indicate more desorption hysteresis, and no desorption hysteresis occurs when HI = 0. The HI values of three conditions in this study at different equilibrium concentrations were calculated and listed in Table 4. The HI values for CV on MWCNTs are less than 0.05, which means that the difference between desorption and adsorption equilibria is within 5%. Thus, no adsorption/desorption hysteresis is considered to exist for adsorption of CV on A-MWCNTs. The HI values of BR9 on O-MWCNTs are higher than those of BR9 on A-MWCNTs. This is because there are more carboxyl groups on O-MWCNTs than on A-MWCNTs, as indicated by FTIR analysis, which results in more irreversible amidation for BR9 on O-MWCNTs than on A-MWCNTs. Similar results have been observed for the adsorption/desorption hysteresis of aniline and 4-methylaniline on MWCNTs (Wu *et al.* 2013).

The HI value decreases with increasing equilibrium concentration in all three systems. For example, adsorption/desorption hysteresis of BR9 on O-MWCNTs is the greatest, and the HI values are 1.36, 0.75, and 0.22 when the equilibrium concentrations are 10 mg/L, 20 mg/L, and 50 mg/L, respectively. As mentioned previously, amidation might limit the access of BR9 to the inner grooves. At high concentration, the inner grooves might be quickly blocked, and most of the adsorption occurs on the exterior surface. Those BR9 molecules adsorbed via π–π interaction on the exterior surface can thus desorb easily. As the concentration decreases, the blockage of the inner surface due to amidation may also be limited in the beginning stage of adsorption. Thus, more BR9 molecules may transport into

Table 4 | HI values of CV and BR9 on MWCNTs at different equilibrium concentrations

	HI 10 mg/L	HI 20 mg/L	HI 50 mg/L
CV (A)	0.05	0.02	0.00
BR9 (A)	0.83	0.39	0.05
BR9 (O)	1.36	0.75	0.22

the pores and may be difficult to desorb if those pores are blocked in the later stage of the adsorption.

CONCLUSIONS

The adsorption and desorption of CV and BR9 on MWCNTs were conducted to investigate adsorption and desorption mechanisms. The adsorption kinetics could be described by the pseudo-second-order model, suggesting that the interaction between CV, as well as BR9, and the surface of MWCNTs is the rate-limiting step. The adsorption and desorption of CV and BR9 follow the Langmuir model; however, the mechanisms differ. The π–π interaction dominates the adsorption and desorption of CV on A-MWCNTs, and the additional irreversible bonding and steric hindrance significantly affect the transports and equilibria of adsorption and desorption of BR9 on both A- and O-MWCNTs. The adsorption/desorption kinetics also support the conclusions of adsorption/desorption isotherms and hysteresis. Amidation leads to slower adsorption equilibrium, lower adsorption capacity, and more significant adsorption/desorption hysteresis. These results show that the structural and chemical properties of organic compounds play significant roles in their interactions with CNTs. These findings may also provide additional information with respect to the fate and transport of both carbonaceous nanomaterials and organic pollutants in aquatic environments. Solution pH and ionic strength may also affect the adsorption due to dissociation of adsorbates and functional groups on MWCNTs, which may affect the hydration bonding, steric hindrance, and electrostatic interactions. The effects of solution pH and ionic strength may be considered in the future to better explore the adsorption/desorption phenomena.

REFERENCES

Agnihotri, S., Mota, J. P. B., Rostam-Abadi, M. & Rood, M. J. 2005 Structural characterization of single-walled carbon nanotube bundles by experiment and molecular simulation. *Langmuir* **21**, 896–904.

Apul, O. G. & Karanfil, T. 2015 Adsorption of synthetic organic contaminants by carbon nanotubes: a critical review. *Water Research* **68**, 34–55.

Chi, M.-F., Wu, W.-L., Du, Y., Ching-Ju, C. & Chu-Ching, L. 2016 Inactivation of Escherichia coli planktonic cells by multi-walled carbon nanotubes in suspensions: effect of surface functionalization coupled with medium nutrition level. *Journal of Hazardous Materials* **318**, 507–514.

Chin, C.-J. M., Shih, M.-W. & Tsai, H.-J. 2010 Adsorption of nonpolar benzene derivatives on single-walled carbon nanotubes. *Applied Surface Science* **256** (20), 6035–6039.

Gotovac, S., Honda, H., Hattori, Y., Takahashi, K., Kanoh, H. & Kaneko, K. 2007 Effect of nanoscale curvature of single-walled carbon nanotubes on adsorption of polycyclic aromatic hydrocarbons. *Nano Letters* **7** (3), 583–587.

Ho, Y. S. & McKay, G. 1999 Pseudo-second order model for sorption processes. *Process Biochemistry* **34**, 451–465.

Huang, W., Yu, H. & Weber, W. J. J. 1998 Hysteresis in the sorption and desorption of hydrophobic organic contaminants by soils and sediments 1. A comparative analysis of experimental protocols. *Journal of Contaminant Hydrology* **31**, 129–148.

Jin, Z., Wnag, X., Sun, Y., Ai, Y. & Wang, X. 2015 Adsorption of 4-n-nonylphenol and bisphenol-A on magnetic reduced 2 graphene oxides: a combined experimental and theoretical studies. *Environmental Science & Technology* **49**, 9168–9175.

Kuo, C.-Y. 2009 Comparison with as-grown and microwave modified carbon nanotubes to removal aqueous bisphenal A. *Desalination* **249**, 976–982.

Lagergren, S. 1998 About the theory of so-called adsorption of soluble substances. *Kungliga Svenska Vetenskapsakademiens Handlingar* **24**, 1–39.

Lin, D. & Xing, B. 2008 Adsorption of phenolic compounds by carbon nanotubes: role of aromaticity and substitution of hydroxyl groups. *Environmental Science & Technology* **42** (19), 7254–7259.

Liu, W., Jiang, X. & Chen, X. 2015 Synthesis and utilization of a novel carbon nanotubes supported nanocables for the adsorption of dyes from aqueous solutions. *Journal of Solid State Chemistry* **229**, 342–349.

Ma, X., Anand, D., Zhang, X. & Talapatra, S. 2011 Adsorption and desorption of chlorinated compounds from pristine and thermally treated multiwalled carbon nanotubes. *The Journal of Physical Chemistry C* **115** (11), 4552–4557.

Madrakian, T., Afkhami, A., Ahmadi, M. & Bagheri, H. 2011 Removal of some cationic dyes from aqueous solutions using magnetic-modified multi-walled carbon nanotubes. *Journal of Hazardous Materials* **196**, 109–114.

McKay, G., Ho, Y. S. & Ng, J. C. Y. 1999 Biosorption of copper from waste waters: a review. *Separation and Purification Reviews* **28**, 87–125.

Oleszczuk, P., Pan, B. & Xing, B. 2009 Adsorption and desorption of oxytetracycline and carbamazepine by multiwalled carbon nanotubes. *Environmental Science & Technology* **43**, 9157–9173.

Pan, B., Lin, D., Mashayekhi, H. & Xing, B. 2008 Adsorption and hysteresis of bisphenol A and 17r-ethinyl estradiol on carbon nanomaterials. *Environmental Science & Technology* **42**, 5480–5485.

Sabna, V., Thampi, S. G. & Chandrakaran, S. 2016 Adsorption of crystal violet onto functionalised multi-walled carbon nanotubes: equilibrium and kinetic studies. *Ecotoxicology and Environmental Safety* **134**, 390–397.

Salam, M. A. & Burk, R. C. 2008 Thermodynamics of pentachlorophenol adsorption from aqueous solutions by oxidized multi-walled carbon nanotubes. *Applied Surface Science* **255**, 1975–1981.

Saleh, N. B., Pfefferle, L. D. & Elimelech, M. 2008 Aggregation kinetics of multiwalled carbon nanotubes in aquatic systems: measurements and environmental implications. *Environmental Science & Technology* **42**, 7963–7969.

Shek, T., Ma, A., Lee, V. & McKay, G. 2009 Kinetics of zinc ions removal from effluents using ion exchange resin. *Chemical Engineering Journal* **146**, 63–70.

Tsai, R. S., el Tayar, N. E. & Testa, B. 1991 Toroidal coil centrifugal partition chromatography, a method for measuring partition coefficients. *Journal of Chromatography* **538**, 119–123.

Wang, X., Liu, Y., Qiu, W. & Zhu, D. 2002 Immobilization of tetra-tert-butylphthalocyanines on carbon nanotubes: a first step towards the development of new nanomaterials. *Journal of Materials Chemistry* **12** (6), 1636–1639.

Wang, X., Liu, Y., Tao, S. & Xing, B. 2010a Relative importance of multiple mechanisms in sorption of organic compounds by multiwalled carbon nanotubes. *Carbon* **48** (13), 3721–3728.

Wang, Z., Yu, X., Pan, B. & Xing, B. 2010b Norfloxacin sorption and its thermodynamics on surface-modified carbon nanotubes. *Environmental Science & Technology* **44**, 978–984.

Weber, W. J. & Morris, J. C. 1963 Kinetics of adsorption on carbon solution. *Journal of the Sanitary Engineering Division by American Society of Civil Engineers* **89**, 31–59.

Wu, W., Jiang, W., Zhang, W., Lin, D. & Yang, K. 2013 Influence of functional groups on desorption of organic compounds from carbon nanotubes into water: insight into desorption hysteresis. *Environmental Science & Technology* **47** (15), 8373–8382.

Yang, K. & Xing, B. 2007 Desorption of polycyclic aromatic hydrocarbons from carbon nanomaterials in water. *Environmental Pollution* **145** (2), 529–537.

Yang, K., Wu, W., Jing, Q., Jiang, W. & Xing, B. 2010 Competitive adsorption of naphthalene with 2,4-dichlorophenol and 4-chloroaniline on multiwalled carbon nanotubes. *Environmental Science & Technology* **44**, 3021–3027.

Yu, S., Wang, X., Yao, W., Jian, W., Ji, Y., Ai, Y., Alsaedi, A., Hayat, T. & Wang, X. 2017 Macroscopic, spectroscopic and theoretical investigation for the interaction of phenol and naphthol on reduced graphene oxide. *Environmental Science & Technology* **51**, 3278–3286.

First received 25 July 2018; accepted in revised form 21 April 2019. Available online 2 May 2019